Research Article | Vol. 29, No. 6 / 15 March 2021 / Optics Express 9532
Optics EXPRESS

Observation of split evanescent field distributions in tapered multicore fibers for multiline nanoparticle trapping and microsensing

DONG YAN,[1] ZHEN TIAN,[1,2] NAN-KUANG CHEN,[1,5] LIQIANG ZHANG,[1,6] YICUN YAO,[1] YANRU XIE,[1] PERRY PING SHUM,[3] KENNETH T. V. GRATTAN,[4] AND DAQIN WANG[1]

[1]*School of Physics Sciences and Information Technology, Liaocheng University, Liaocheng 252000, China*
[2]*State Key Laboratory of Information Photonics and Optical Communications, Beijing University of Posts and Telecommunications, Beijing 100876, China*
[3]*Department of Electrical and Electronic Engineering, Southern University of Science and Technology, Shenzhen 518055, China*
[4]*Department of Electrical and Electronic Engineering, City, University of London, London EC1 V 0HB, United Kingdom*
[5]*nankuang@gmail.com*
[6]*zhangliqiang@lcu.edu.cn*

Abstract: The optical attractive force in tapered single-mode fibers (SMFs) is usually uniformly distributed around the tapered section and has been found to be important for trapping and manipulating targeted atoms and nanoparticles. In contrast, a peculiar phenomenon of the evanescent field splitting along the azimuth axis can be experimentally observed by tapering a weakly-coupled MCF into a strongly-coupled MCF to generate supermode interference. Moreover, the supermode interference produces a hexagonally distributed evanescent field and its six vertices give rise to the multiline optical attractive force. For such spectral resonances, the optimum extinction ratio for the transmission dips is given by 47.4 dB, this being determined using an index liquid to cover the tapered MCF. The resonant dips move to a greater extent at longer wavelengths, with the optimum tuning efficiency of 392 nm/RIU for index sensing. The split evanescent fields respectively attract the excited upconversion nanoparticles in the liquid to be linearly aligned and running down the tapered region over the fiber surface, emitting green light with 60° symmetry. The charged nanoparticles were periodically self-organized, with a period of around 1.53 μm. The parallel lines, with 60° rotational symmetry, can be useful for (1) indicating the exact locations of the side-cores or orientations of the tapered MCF; (2) as precision alignment keys for micro-optical manipulation; and (3) enhancing the upconversion light, or for use in lasers, coupling back to the MCF. The split evanescent fields can be promising for developing new evanescent field-based active and passive fiber components with nano-structures.

1. Introduction

Many different kinds of the active and passive fiber components can be used as building blocks in fiber optic systems, for making filters, couplers, multiplexers, interferometers, sensors, amplifiers and lasers. To interact with the guiding light in the fiber core, several different approaches have been proposed, including intra-core components based on laser inscribing [1], functional ion-doping into the core [2], material filling the air holes in photonic crystal fibers or hollow band-gap fibers [3,4], thin film coating at the fiber cleaved end [5] and evanescent field coupling [6,7]. For evanescent field coupling, the major fabrication methods used are side-polishing, chemical-etching, laser-ablation and fused-tapering [8–11]. The external functional materials

#419194 https://doi.org/10.1364/OE.419194
Journal © 2021 Received 11 Jan 2021; revised 24 Feb 2021; accepted 6 Mar 2021; published 11 Mar 2021

Optics EXPRESS

used are usually placed in the evanescent field region, to change the optical characteristics of the guided light. The distance and the interaction length of the evanescent field, seen against the external material, are crucial issues for achieving either high sensitivity or high-performance efficiency. Generally, for active or passive components made of fused-tapered SMFs, the evanescent field distribution is rotationally symmetric, along the azimuth axis, with the magnitude of the electric field exponentially decaying along the radial axis, and outwardly [11]. When the laser light is sufficiently strong, the use of the optical attractive force can be an effective way to manipulate molecules or nanoparticles, in the evanescent field region [12].

However, in contrast to a tapered SMF, a tapered MCF has a very different wave-guiding structure – one in which the high index 'side cores' are periodically distributed and surrounding the central core, forming a strongly-coupled MCF structure to allow generating supermodes [13–16], suitable for sensing applications [17,18]. However, it can be experimentally observed here that the hexagonal evanescent field leads to a rotationally-dependent power distribution, which can be observed for the excited supermodes in a seven-core tapered MCF, when the fundamental mode only is launched from its central core. During tapering, the weakly-coupled MCF becomes a strongly-coupled MCF, which then can excite the hexagonally symmetric supermodes when the periodically-distributed 'side cores' are moved to enter the effective mode area of the central core. The spectral oscillations from the supermode interferences [15] are similar to those seen for long period gratings (LPGs) [19,20]. For the first time, this phenomenon of rotationally split evanescent fields is found and been exploited to increase the number of sensing parameters considered, using various micro-structured devices mounted on a tapered MCF, offering the flexibility to adjust the relative rotational positions. It can also attract nanoparticles, to precisely identify the exact location of the tapered side cores and the orientation of the tapered MCF, to create precision alignment keys with a 60° rotational symmetry for micro-optic manipulation, to enhance the coherent upconversion radiation, or potentially allow laser action, this being emitted from the attracted, then aligned nanoparticles or nanocrystals.

2. Working principle of the split evanescent fields and fundamentals of the optical trapping force

For the weakly-coupled MCF used in this work, the core diameter, d_1, was 5.62 μm (and this was almost identical for the seven cores considered). The distance between each core has been carefully designed to avoid power cross-coupling. Figure 1(a) shows the dimensions of the fiber used, where d_2 and d_3 are given by ~29.4 μm. The laser light from the SMF was launched into the central core (through fusion splicing) and thus confined to propagate only along the central core, with the six side cores not being excited. Since the weakly-coupled MCF has a numerical aperture (NA) as high as 0.2, the splicing point between the MCF and the SMF (SMF-28) will excite high order core modes, which makes our further investigation ambiguous on the supermode interference effect. Therefore, to avoid exciting the higher order core modes, two kinds of SMFs (with NA = 0.15 and 0.2), both with a length of 1.5 meters, were respectively inserted in order, between the MCF and the SMF. With the help of this transition in the NA, the excitation of the high order core modes can be efficiently suppressed. When the weakly-coupled MCF was heated and tapered the six, then tapered, side cores gradually overlap with the effective mode area of the tapered central core, to form a strongly-coupled MCF structure, which then can excite two supermodes and generate supermode interference as a result [15]. These interference effects can be further enhanced as the tapered waist D decreases, to generate several transmission dips. Thus, approaching a value of 35 μm, the evanescent fields available at the tapered waist of the tapered MCF become much more rotationally dependent. This phenomenon was observed in the one cross-sectional microphotograph of the fiber (taken using a 1000x CCD microscope) we had, showing the supermode at the taper waist (D = 30 μm). However, the picture is not shown in this paper, due to its poor pixel quality and we were not able to take another picture.

Optics EXPRESS

Shown schematically in Fig. 1(b), the cores and the optical power intensity distribution are respectively represented in yellow and green. When the refractive index (n) calibration liquids (n> 1.35 and varying over the range 1.351-1.452) cover the position of the evanescent field, the resonant wavelengths all start to move toward longer wavelengths. Figures 1(c)–1(d) show schematics of the index profiles of the tapered MCF along the A and B axes respectively, as can be seen from Fig. 1(a). The role the six side cores play is similar to the W-index profile in dispersion compensated fiber [21,22], where the effective index curve becomes more dispersive at longer (rather than shorter wavelengths), thus to provide, in an efficient way, a larger, high order dispersion compensation. Accordingly, the resonant wavelengths change more rapidly at these longer wavelengths, due to the more expanded evanescent fields. This phenomenon becomes more obvious when using external liquids of higher refractive index, indicating that the sensitivity can be improved significantly at these longer wavelengths. In addition, the resonant wavelength red-shifts with increasing ambient index. This is very different from the conventional fiber interferometers such as Mach-Zehnder. To consider two excited supermodes, the intensity of the interference can be expressed as Eq. (1).

$$I = I_{S_1} + I_{S_2} + 2\sqrt{I_{S_1} I_{S_2}} \cos\left(\frac{2\pi L \Delta n_{eff}}{\lambda}\right) \tag{1}$$

where I_{S_1} and I_{S_2} are the intensity for the 1st supermode (lower-order mode) and the 2nd supermode (higher-order mode), respectively. λ is the operating wavelength and L is the interference length. The term Δn_{eff} represents the difference between the effective indices of the 1st and the 2nd supermodes, respectively. The resonant dips λ_m, shown in Eq. (3), occur at the destructive interference conditions when $2\pi\Delta n_{eff}/\lambda = (2m+1)\pi$ is satisfied [23]. By differentiating the λ_m with respect to the ambient index, n, it is found that $\Delta N = \partial n_{eff}^{S_1}/\partial n - \partial n_{eff}^{S_2}/\partial n$, as shown in Eq. (4). When n increases, the value of $n_{eff}^{S_2}$ decreases since the evanescent field gradually leaves the high index side cores and extends more outside the tapered MCF. This gives rise to an increasing value of ΔN and which makes the resonant wavelengths red-shift.

$$\Delta n_{eff} = n_{eff}^{S_1} - n_{eff}^{S_2} \tag{2}$$

$$\lambda_m = \frac{2L\Delta n_{eff}}{2m+1} \tag{3}$$

$$\frac{\partial \lambda_m}{\partial n} = \left(\frac{2L}{2m+1}\right)\left(\frac{\partial n_{eff}^{S_1}}{\partial n} - \frac{\partial n_{eff}^{S_2}}{\partial n}\right) = \frac{2L}{2m+1}\Delta N \tag{4}$$

To confirm that the evanescent field is indeed split due to the multicore structures, some simulations were undertaken simultaneously. The mode field distributions were simulated by considering the tapered diameter of 57 μm, where the indices of the core and cladding were 1.459 and 1.444, respectively, at the working wavelength of 1550 nm, based on the use of the Beam Propagation Method, using Rsoft2020. The 2D and 3D mode field distributions are respectively shown as the hexagonal dotted white lines in Figs. 1(e)–1(g). For D = 35 μm, the 2D and 3D mode field distributions are respectively shown in Figs. 1(g) and 1(h). It is obvious that the evanescent field is rotationally dependent along the azimuth axis. In Figs. 1(e) and 1(g), the cyan solid circular lines are the physical boundary of the tapered MCF. Clearly, the generated optical trapping force in Fig. 1(e) will be higher than that in Fig. 1(g), since the magnitude of the electric field varies more heavily along the azimuth axis on the cyan circular line. In Fig. 1(g), the electric field penetrates more outside the tapered MCF, which makes the gradient trapping force decrease on the cyan circle.

For the split evanescent fields based on supermode interference in this tapered MCF, it is interesting to investigate the optical attractive force, namely the near-field trapping force

Optics EXPRESS

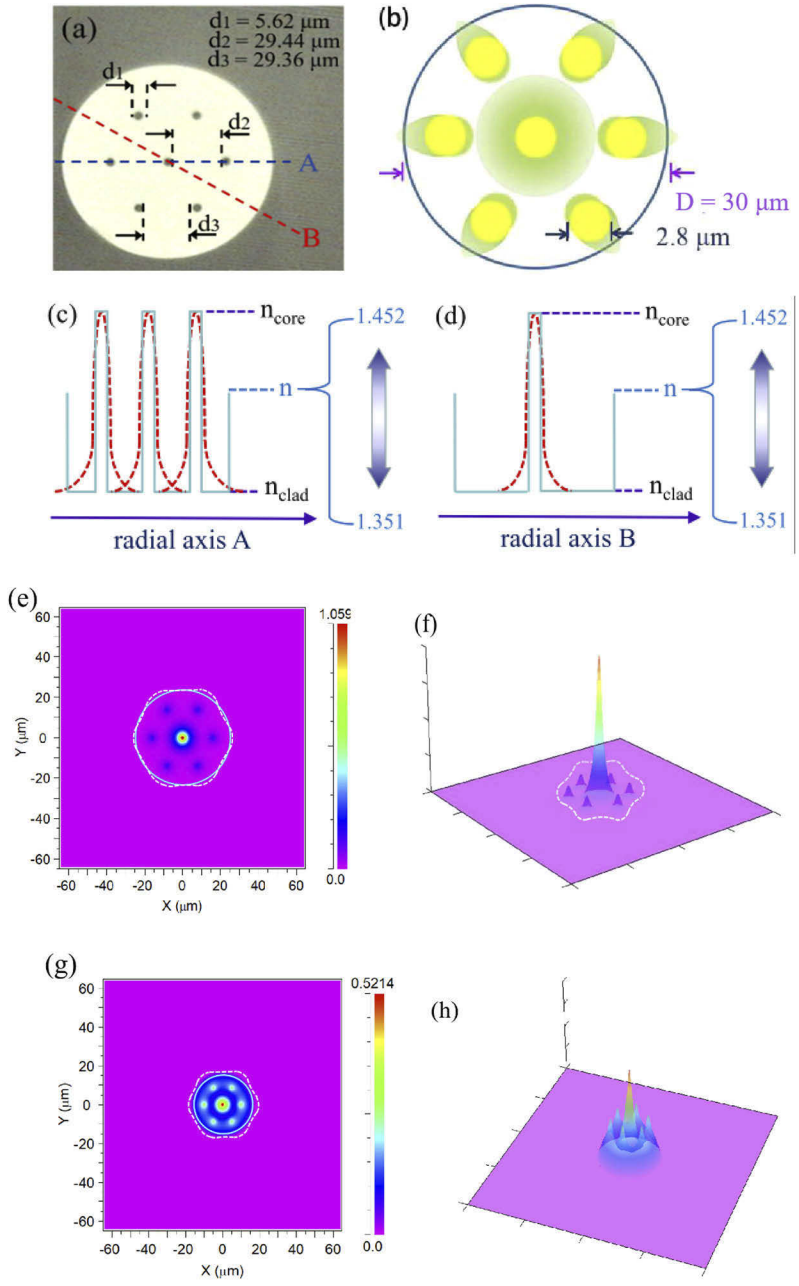

Fig. 1. (a) Schematic of the multi-core fiber and (b) optical power intensity distribution for the tapered MCF and the supermode at a tapered waist (D = 30 μm) together with a schematic illustration of the rotationally dependent optical power intensity distribution of the strongly-coupled tapered MCF. Schematics of the refractive index profiles of the tapered MCF along the (c) A and (d) B axes, respectively (as seen from (a)). The index n of ambient liquids used ranges from 1.351 to 1.452. The simulated mode field distribution for (e) 2D (D = 57 μm), and (f) 3D (D = 57 μm), and (g) 2D (D = 35 μm), and (h) 3D (D = 35 μm) at 1550 nm wavelength.

Optics EXPRESS

[11,24–26], in this tapered MCF. In fact, in a tapered SMF, the evanescent wave, namely the fast decaying electric field, of the guiding light penetrates the cladding into the external medium to generate a gradient force. It can be used to attract micro- and nano-particles toward the tapered fiber for evanescent particle trapping, binding [27], propulsion and transportation [24–28], this being contingent upon the laser input power. To enhance the gradient force, it is essential to achieve a rapidly decaying electric field using a waveguide with high index contrast or a suitable tapered waist diameter, D. From Figs. 1(e) and 1(g), it is found that the electric field generates the higher optical gradient force when D is at ~57 μm, more so than at ~35 μm. This arises because a larger D can lead to a sharper electric field distribution across the tapered fiber and air interface. However, in this work, it is noted that the nano-particles trapping can be experimentally observed only within the D range, 30-60 μm. When D is larger than 60 μm, the evanescent field is insufficient to attract the nano-particles. When D is smaller than 30 μm, the evanescent field decay slowly and therefore the gradient force is negligible. It is straightforward to note that, based on the same physical concept, the gradient force deriving from the split evanescent fields will be also split along the azimuth axis. Obviously, the effect of nano-particle trapping is one of the best methods to verify this physical phenomenon. For such a novel observation, the nano-particles can be self-organized and self-aligned, which could be very useful to investigate the phenomenon of nano-lasers, using particles with chromophores or gain media. It can also open a new method for particle manipulation and for multi-parameter microsensing applications.

3. Device fabrication and nanoparticle trapping for enhanced upconversion lights

The weakly-coupled MCF (FIBERCORE) used in this work was designed for use with operating wavelengths in the C-band, where the diameters for the core, cladding, and mode field were 5.62 μm, 124.5 μm, and 6 μm, respectively. The second mode cut-off wavelength was 1342 nm and the NA was 0.2. The indices for the core (n_{core}) and the cladding (n_{clad}) were in the range 1.4578 to 1.4607 and 1.444 (at 1550 nm) respectively. The worst geometric mis-location of a core experienced was 1.2 μm. Investigating the influence of the periodically distributed Ge-doped core (with a 60° rotational symmetry), a light source in the spectral region 1250 to 1650 nm, with a spectral power density >−25 dBm from multiple superluminescent diodes (SLDs) was used, launching light into the central core through the SMF. Flame tapering enabled the central core in the MCF to be gradually shrunk to expose its mode field, to form a strongly-coupled MCF in which two supermodes in this axially symmetric SMF-MCF-SMF structure were excited [15]. The hydrogen flame torch, scanning back and forth for achieving adiabatic tapering, was carried by a precision stepping motor to heat and stretch the fiber until a desired tapered diameter was reached based on program-controlled tapered fiber workstation. The hexagonally symmetric mode pattern at the taper waist (D = 60.2 μm) that was achieved is shown in Fig. 2(a) (1000x magnification CCD microscope). Figure 2(a) clearly shows that the supermodes are actually a combination of the LP modes supported by each MCF core [13–16] (silicon detectors used in the CCD microscope used are sensitive below ~1350 nm). The 30-cm-long MCF (before the tapered region and including the splicing point) was coiled to a radius, R_1, of 3 cm, to remove any excited high order core modes possible. The intensity mode pattern of the other excited supermode is shown in Fig. 2(b) (where R_1 was decreased to 1.5 cm).

Figure 2(c) shows the experimental setup for investigating the optical attractive force for the hexagonal evanescent field of the tapered MCF, fabricated by using flame tapering, while the SLD is used as the light source for measuring supermode interferences, as described earlier. Two kinds of coiled SMFs (with NA = 0.15 and 0.2 respectively), both with a length of 1.5 meters, were inserted in that order between the MCF and the SMF, to suppress the excitation of the higher order core modes, as shown in Fig. 2(c) and as mentioned earlier in Section 2. In the block with the dotted line, the experimental setup for measuring the excited upconversion purple/green/red light coupling back to the tapered MCF is shown. They are further clearly separated by a blazed

Optics EXPRESS

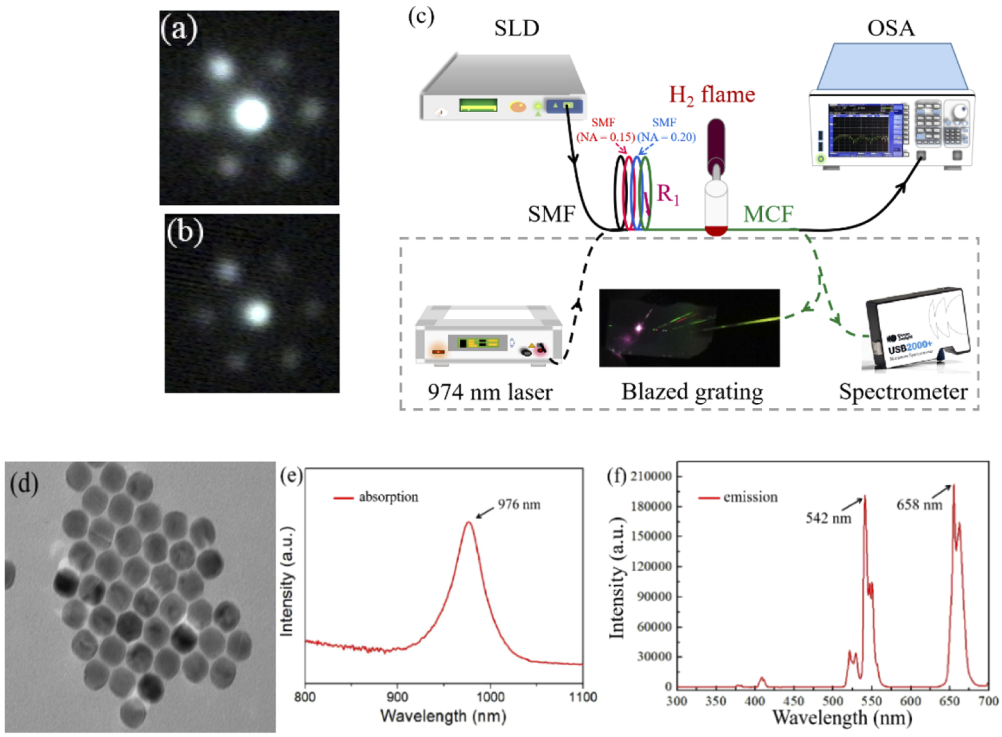

Fig. 2. Intensity distributions of the supermode at the taper waist (D = 60.2 μm) when R_1 was (a) 3 cm and (b) 1.5 cm. (c) Experimental set-up. (d) SEM picture and (e) absorption and (f) emission spectra of the Er^{3+}/Yb^{3+}-sensitized $NaYF_4$ nanoparticles.

grating, backwardly inclined at 45°, and the spectrum was recorded by using a spectrometer covering the wavelength range of 350-1000 nm. The upconversion fluorescence nanoparticles were Er^{3+}/Yb^{3+}-sensitized $NaYF_4$, where the SEM picture shows that each nanoparticle has a hexagonal shape [in Fig. 2(d)], with average lengths for the diagonal and the side length of 35.31 nm and 16.37 nm, respectively. The strongest absorption occurs at 976 nm, while the major emission peaks, located at 542 nm and 658 nm, are shown in Figs. 2(e) and 2(f), respectively. To verify the hexagonal evanescent field distribution, light from a 1550 DFB laser with an output power of 77 mW, amplified by an erbium-doped fiber amplifier, was launched into the central core of a tapered MCF, this being immersed in the liquid with dispersed upconversion nanoparticles for about 2 minutes to attract the nanoparticles attaching onto the extremely localized area along the split evanescent fields. The tapered MCF was then moved from the liquid to the air.

From Figs. 3(a)–3(e), it can be seen that at the different viewing angles used (0°, 30°, 60°, 300°, and 330°) in the air the nanoparticles are attracted by the optical attractive force deriving from the hexagonal evanescent fields of the supermode, (shown in Fig. 2(b) under a CCD microscope of 1000x magnification). The clustered nanoparticles gather together to form a dot with a diameter of ~3 μm. The nanoparticle dots align with each other very accurately to form three parallel, 60° rotationally symmetric lines, running along the tapered MCF, using sample A, and are excited by the 1550 nm to emit very weak green upconversion light, (which was seen as a weak green light with the naked eye in a dark room but was observed as white under a CCD microscope of 1000x magnification due to an incorrect white balance in the instrument). The sample A has a tapered waist of D = 48.75 μm and a tapered length of 17 mm, respectively. In addition, the distance t_1 (light blue lines and words) between the two neighboring fluorescent lines increases

Optics EXPRESS

with increasing D (yellow lines and words), shown in Fig. 3(f), using sample B with a tapered waist of D = 36.75 μm and tapered length of 19 mm. The nanoparticles, which were attracted, are self-organized with a period of 1.53 μm, and tightly adhered to the surface of the tapered MCF, when it then was violently and repeatedly twisted/untwisted until broken. The adhering nanoparticles could only be removed by vigorous rubbing using a paper wetted with alcohol and used as a wipe. This presents strong evidence to show that the evanescent power of the supermode is axial, rotationally, this being dependent on the near-field region.

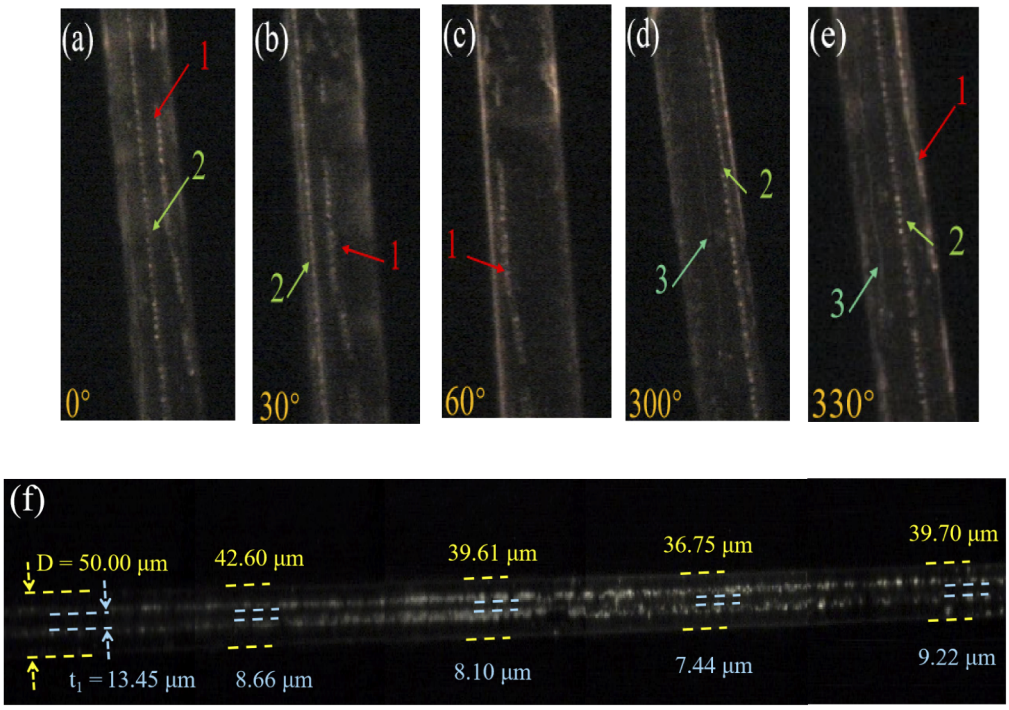

Fig. 3. (a)-(e) Micrographs of the tapered MCF with aligned upconversion nanoparticles to form 60° rotational symmetric lines at different viewing angles, under a CCD microscope of 1000x magnification. (f) Microphotograph of the tapered MCF in which the distance t_1 (light blue lines and words) between two neighboring nanoparticle lines increases with increasing tapered diameter D (yellow lines and words), under a CCD microscope of 1000x magnification.

To investigate whether or not the upconversion light will be coupling back to the MCF from the aligned nanoparticles, a 974 nm pump light (at 90 mW) was launched into the tapered MCF. However, the generated upconversion light was very weak due to the tiny amount of the trapped nanoparticles on the tapered MCF, the upconversion light coupling back to propagate along the core of the MCF and the following 1-meter-long standard C-band SMF, becomes too lossy to be observed. To conquer this issue, the MCF was then cleaved at a position 3 cm away from the rear edge of the tapered transition so as to allow a successful measurement of the spectrum of upconversion light using a spectrometer (designed for visible and near-infrared use). In addition, the distance of 3 cm away from the tapered region is helpful to avoid most of the stray light from the illuminating aligned nanoparticles on the tapered MCF and confirm the measured spectra were actually the upconversion light, coupling back to propagate in core of the un-tapered MCF. A blazed grating, of 600 lines/mm, with its length and width of 25 mm and 10 mm, respectively, was then backwardly inclined at 45° and placed after the cleaved MCF to diffract the exciting

Optics EXPRESS

purple/green/red and pump light, shown in Fig. 4(a), using a cellphone camera. In Fig. 4(a), at the bottom, the green light is the MCF with the guiding upconversion and residual pump light. The green, red, and pump (974 nm) light are respectively diffracted and observed from the bottom to the top. Since the blazed grating was designed for a wavelength of 1000 nm, the multiple green light beams at different positions can thus be found to be due to high order diffraction. The residual pump light was much stronger than the upconversion light and a brighter spot can thus be observed from the blazed grating. To measure the spectral responses from the upconversion light, the pump power at 974 nm was reduced to 20 mW to avoid damaging the spectrometer (Ocean Optics: USB2000+). The measured spectrum was shown in Fig. 4(b) and the peak wavelengths for the purple/green/red light beams are 391.05 nm, 582.59 nm, and 782.93 nm, respectively. The purple light could not be shown in Fig. 4(a) because it was blocked by the cellphone camera. In contrast to the upconversion light beams, the 974 nm pump light was too strong to be shown with its peak. Interestingly, the linewidth of those upconversion light beams in Fig. 4(b) are much narrower than that of the emission spectrum in Fig. 2(f). Importantly, the aligned nanoparticles along with the split evanescent fields can be helpful to make nano-lasers using nanoparticles. In short, the multiline aligned nanoparticles can be useful for several reasons (1) to precisely indicate the exact locations, at the middle position between two neighboring nanoparticle lines, of the tapered side cores and the orientation of the MCF; (2) to play a role as precision alignment keys for micro-optical manipulation; and (3) to enhance the upconversion radiation coupling back to the MCF. Usually, the lifetime of the electrons occupying the excited states for visible, upconversion light is within a few hundreds of microseconds, thus the coherent photons could be amplified to generate upconversion laser action, when the clustered nanoparticles are self-organized and well-aligned to achieve a linear laser cavity, in this way to improve the laser signal-to-noise ratio using this method.

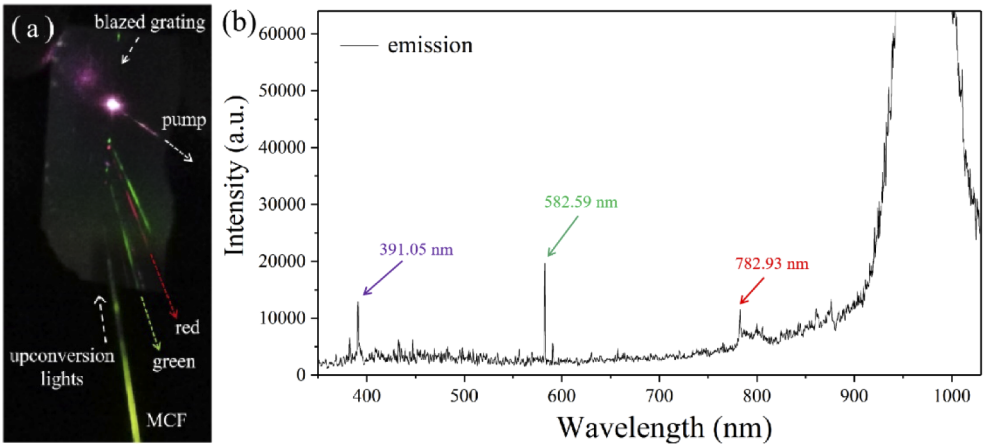

Fig. 4. (a) The upconversion green and red lights as well as the 974 nm pump lights are separated by a blazed grating at an inclined angle of 45°. (b) Measured spectrum for the upconversion purple/green/red and pump (974 nm) lights.

4. Experimental results and discussion for index sensing

Apart from using nanoparticle trapping for enhancing the upconversion light due to the split evanescent fields of the tapered MCF, it is also interesting to investigate their other potential applications in index sensing based on the supermode interference associated with the tapered MCF. In Fig. 5(a), the spectra obtained are shown, where the gray, green, blue/cyan, and red lines represent the spectral responses for the SLD and the normalized transmission losses for

Optics EXPRESS

the tapered MCFs, with values of D = 65 μm, 55 μm, and 42 μm, respectively (under an optical resolution of 0.05 nm, observed using a OSA). The gray line shows the multiple comb-like dips ranging over the wavelength range 1350-1450 nm and which arise from the water vapor absorption in the hygroscopic monochromator of the OSA (Yokogawa: AQ6370D). During the tapering process, small power oscillations in the spectra start to be observed when D approaches 65 μm, since the supermodes are excited and thus will generate interference. Further 'thinning down' the MCF (and thus reducing its diameter) allows more and more dips to be generated, with growing extinction ratios, as shown in Fig. 5(a). When D reaches a value of 55 μm, the spectral responses are almost the same, no matter whether the tapered MCF is in air or immersed in the index liquid (n = 1.393). Thus, the evanescent field of the tapered MCF is still not accessible (from the experimental results, the evanescent field becomes accessible when D reaches a value of ~35 μm). The spectral responses were investigated by using a series of calibrated refractive index liquids to entirely cover the tapered MCF (prepared by mixing deionized water and glycerin, with a specific weight ratio with the index precisely measured by using an Abbe refractometer with an accuracy to the third decimal place, at 650 nm), as shown in Fig. 5(b). The insertion loss was ~1.5 dB [due to the NA gap between the SMF (NA = 0.13) and the MCF (NA = 0.2)]. As the refractive index changes, the resonant dips move toward the longer wavelengths as the ambient index, n, gradually increases. The phenomena were predicted and explained by the Eqs. (1)–(4) in Section 2, showing the working principle of the split evanescent fields. The optimum extinction ratio achieved was 47.4 dB, at 1625.82 nm. The resonant wavelengths, red-shifted from an increased value of n, will lead to an increasing index change, Δn, between the two supermodes [14]. The wavelength shift is nonlinear with the index variations, as can be seen from Fig. 5(c). The resonant dips at longer wavelengths change more rapidly, with the optimum tuning sensitivity >391.99 nm/RIU, which is higher than has been reported previously in the literature (including for the tapered MCF sensor, Long Period Grating and Fiber Bragg Grating) [18–20]. The tuning sensitivity for systems reported in the literature [18, 19, and 20] are 171.2 nm/RIU (for an index varying from 1.3448 to 1.3774), 312.5 nm/RIU (for an index varying from 1.315 to 1.395), and 231.4 nm/RIU (for an index varying from 1.32 to 1.44), respectively. The wavelength shifts were seen over the wavelength range from 1449.89 nm to 1627.07 nm, with index variations from 1 to 1.452. The high sensitivity was achieved because the effective mode areas of the excited supermodes were expanded at the longer wavelengths, where the RID curves becomes more dispersive, resembling the characteristics of W-index fiber [21,22]. To compare with the previous limited number of reports related to refractive index sensors based on tapered 7 core MCF [29,30], it is found that the MCFs were intensively tapered, had a tapered diameter D < 10 μm, or etched to significantly expose the evanescent field to allow strong overlap interactions with the external materials. This is very helpful to achieve the very high sensitivity needed, especially when a special medium like graphene [24] was used. However, it is not likely to attract nanoparticles due to the poor gradient force in the evanescent field of the fiber sensors. The gradient force in the evanescent field can only be well-established, within a suitable range, when D itself is ranging over 30-60 μm, in this work. The main breakthrough in our index sensor is to generate the gradient force in the evanescent field to attract upconversion nanoparticles to be self-aligned and self-organized, to allow novel index sensing based on the nanolasers in this device structure. On the other hand, with regard to the index sensor reported [18] using 4-core MCF, the core mismatch is associated with the multimode interference effects in the tapered 4-core MCF for index sensing. However, some of the excited high order cladding modes will go through the four high index cores. This leads to a much higher insertion loss and lower extinction ratios, typically less than 10 dB, for the interference spectra. In contrast, the supermodes in the tapered 7 core MCF in this work were excited by turning the weak coupling MCF into a strongly-coupling version. The excited supermodes were more centrally symmetric, which is helpful to produce an extinction ratio as

Optics EXPRESS

high as 47.4 dB, an insertion loss below 2 dB, and a sensitivity of up to 392 nm/RIU, important for index sensing.

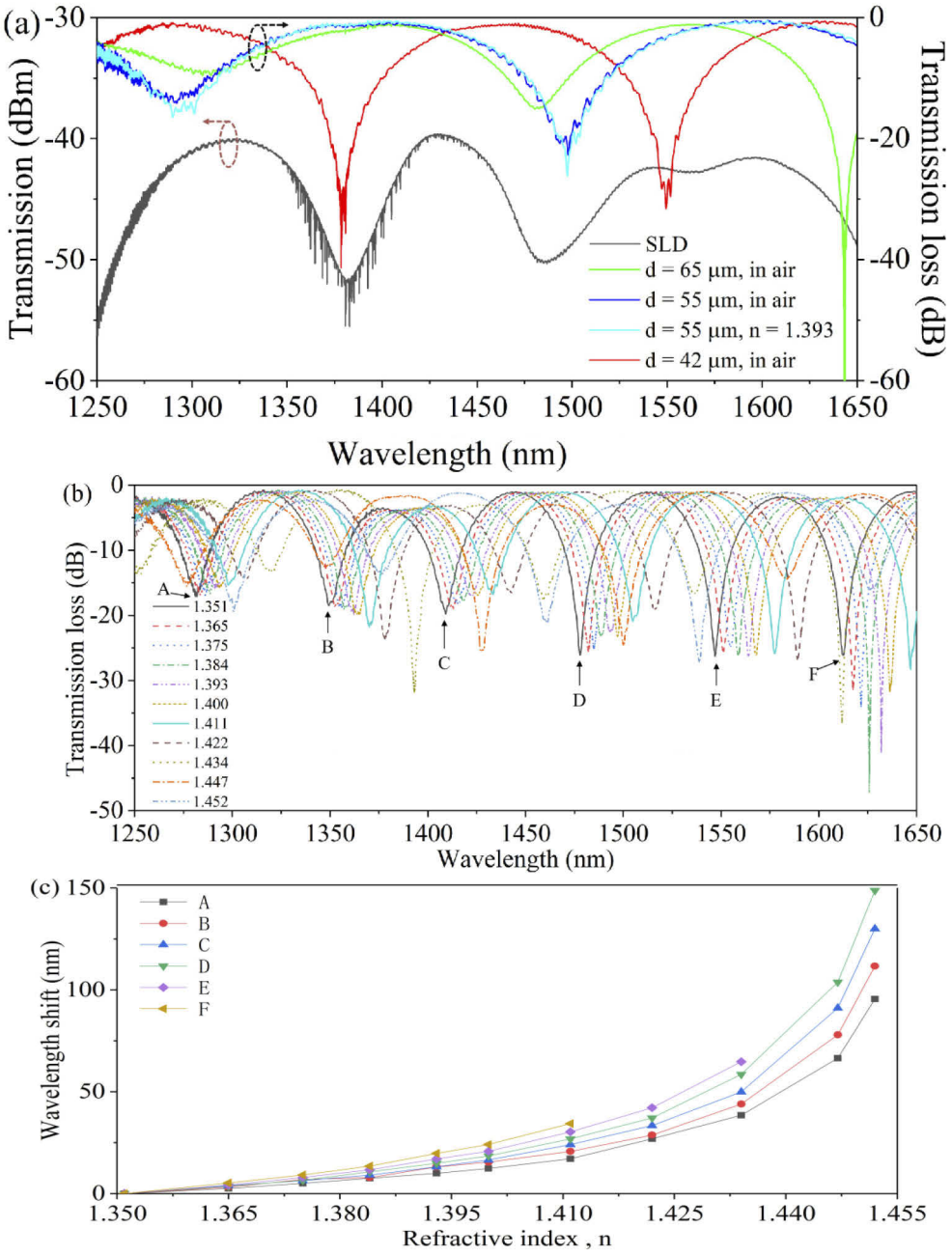

Fig. 5. (a) Spectra of SLD and tapered MCF in air and with varying index liquid overlays, with an optical resolution of 0.05 nm. (b) Spectral response of a tapered MCF (D = 22 μm) at different ambient indices under optical resolution of 0.05 nm. (c) Wavelength shifts versus refractive indices for different transmission dips.

Optics EXPRESS

5. Conclusions

In summary, a tapered MCF with 60° symmetrically distributed high index Ge-doped cores along the azimuthal axis was used to achieve supermode interference, with the best extinction ratio achieved being 47.4 dB; this being suitable for making tunable filters or index sensors. The tapered MCF becomes more dispersive at longer wavelengths, with a nonlinear relationship seen between the wavelength shift observed and the index variations. The optimum wavelength tuning efficiency achieved was 391.99 nm/RIU (for an index varying from 1 to 1.452). For the first time it has been observed that the split hexagonal evanescent field attracts the nanoparticles, causing them to line up running along the tapered MCF, facilitating their use in three potential applications. Thus, they can help (1) precisely to indicate the exact locations of the tapered side cores and the orientation of the tapered MCF; (2) play a role as precision alignment keys with 60° rotational symmetry for micro-optics; and (3) enhance the coherent upconversion radiation, or even allowing for laser action, using emission from the attracted aligned nanoparticles, nanocrystals, or molecules. In contrast to the tapered SMF, this split evanescent field distribution in a tapered MCF along the azimuth axis represents a new method for manipulating nanoparticles and thus is promising for developing new evanescent field passive and active components with multi-parameter micro-sensing.

Funding. Liaocheng University (318051411, 31805180101, 319190301); Natural Science Foundation of Shandong Province (ZR201910210137, ZR201910280068); National Natural Science Foundation of China (61875247).

Acknowledgment. The support of the Royal Academy of Engineering (for Grattan) is greatly appreciated.

Disclosures. The authors declare no conflicts of interests.

References

1. Y. Wang, Z. Li, S. Liu, C. Fu, Z. Li, Z. Zhang, Y. Wang, J. He, Z. Bai, and C. Liao, "Parallel-integrated fiber Bragg gratings inscribed by femtosecond laser point-by-point technology," J. Lightwave Technol. **37**(10), 2185–2193 (2019).
2. H. Li, L. Zhang, R. Sidharthan, D. Ho, X. Wu, N. Venkatram, H. Sun, T. Huang, and S. Yoo, "Pump wavelength dependence of photodarkening in Yb-doped fibers," J. Lightwave Technol. **35**(13), 2535–2540 (2017).
3. V. T. Hoang, R. Kasztelanic, A. Anuszkiewicz, G. Stepniewski, A. Filipkowski, S. Ertman, D. Pysz, T. Wolinski, K. D. Xuan, M. Klimczak, and R. Buczynski, "All-normal dispersion supercontinuum generation in photonic crystal fibers with large hollow cores infiltrated with toluene," Opt. Mater. Express **8**(11), 3568–3582 (2018).
4. R. M. Gerosa, D. H. Spadoti, C. J. S. de Matos, L. d. S. Menezes, and M. A. R. Franco, "Efficient and short-range light coupling to index-matched liquid-filled hole in a solid-core photonic crystal fiber," Opt. Express **19**(24), 24687–24698 (2011).
5. J. Peng, Y. Qu, W. Wang, T. Sun, and M. Yang, "Thin-film-based optical fiber Fabry–Perot interferometer used for humidity sensing," Appl. Opt. **57**(12), 2967–2972 (2018).
6. H. Chen, F. Tian, J. Kanka, and H. Du, "A scalable pathway to nanostructured sapphire optical fiber for evanescent-field sensing and beyond," Appl. Phys. Lett. **106**(11), 111102 (2015).
7. F. Luan, A. K. George, T. D. Hedley, G. J. Pearce, D. M. Bird, J. C. Knight, and P. S. J. Russell, "All-solid photonic bandgap fiber," Opt. Lett. **29**(20), 2369–2371 (2004).
8. N. K. Chen, S. Chi, and S. M. Tseng, "Wideband tunable fiber short-pass filter based on side-polished fiber with dispersive polymer overlay," Opt. Lett. **29**(19), 2219–2221 (2004).
9. N. K. Chen, D. Y. Hsu, and S. Chi, "Widely tunable asymmetric long period fiber grating with high sensitivity using optical polymer on laser-ablated cladding," Opt. Lett. **32**(15), 2082–2084 (2007).
10. K. T. Kim, K. J. Cho, K. Im, S. J. Baik, C. H. Lee, and J. Lee, "High sensitivity refractive index sensor based on a wet-etched fused fiber coupler," IEEE Sens. J. **11**(7), 1568–1572 (2011).
11. N. K. Chen, T. H. Yang, Y. N. Chen, T. Guo, and B. O. Guan, "High sensitivity stretched-abrupt-tapered Mach-Zehnder interferometer with optical attractive force for active microsensing applications," Appl. Phys. Lett. **102**(17), 171101 (2013).
12. M. Ren, H. Cai, L. K. Chin, J. G. Huang, Y. D. Gu, K. Radhakrishnan, W. Ser, and A. Q. Liu, "An opto-mechanical coupled-ring reflector driven by optical force for lasing wavelength control," Appl. Phys. Lett. **108**(8), 081106 (2016).
13. G. Salceda-Delgado, A. V. Newkirk, J. E. Antonio-Lopez, A. Martinez-Rios, A. Schülzgen, and R. Amezcua Correa, "Compact fiber-optic curvature sensor based on super-mode interference in a seven-core fiber," Opt. Lett. **40**(7), 1468–1471 (2015).
14. Y. Jiang, T. Wang, C. Liu, D. Feng, B. Jiang, D. Yang, and J. Zhao, "Simultaneous measurement of refractive index and temperature with high sensitivity based on a multipath fiber Mach-Zehnder interferometer," Appl. Opt. **58**(15), 4085–4090 (2019).

Optics EXPRESS

15. J. Villatoro, O. Arrizabalaga, E. Antonio-Lopez, J. Zubia, and I. S. de Ocariz, "Multicore fiber sensors," OFC 2017, paper no. Th3H.1.
16. C. Xia, M. A. Eftekhar, R. A. Correa, J. E. Antonio-Lopez, A. Schulzgen, and D. Christodoulides, "Supermodes in coupled multi-core waveguide structures," IEEE J. Sel. Top. Quantum Electron. **22**(2), 196–207 (2016).
17. E. Tagoudi, E. K. Milenko, and S. Pissadakis, "Intercore coupling effects in multicore optical fiber tapers using magnetic fluid out-claddings," J. Lightwave Technol. **34**(23), 5561–5565 (2016).
18. C. Zhang, T. Ning, J. Li, L. Pei, C. Li, and H. Lin, "Refractive index sensor based on tapered multicore fiber," Opt. Fiber Technol. **33**, 71–76 (2017).
19. F. Shen, C. Wang, Z. Sun, K. Zhou, L. Zhang, and X. Shu, "Small-period long-period fiber grating with improved refractive index sensitivity and dual-parameter sensing ability," Opt. Lett. **42**(2), 199–202 (2017).
20. X. Fang, C. R. Liao, and D. N. Wang, "Femtosecond laser fabricated fiber Bragg grating in microfiber for refractive index sensing," Opt. Lett. **35**(7), 1007–1009 (2010).
21. F. Gérôme, J. L. Auguste, and J. M. Blondy, "Design of dispersion-compensating fibers based on a dual-concentric-core photonic crystal fiber," Opt. Lett. **29**(23), 2725–2727 (2004).
22. B. J. Mangan, J. Arriaga, T. A. Birks, J. C. Knight, and P. S. J. Russell, "Fundamental-mode cutoff in a photonic crystal fiber with a depressed-index core," Opt. Lett. **26**(19), 1469–1471 (2001).
23. E. Li, "Sensitivity-enhanced fiber-optic strain sensor based on interference of higher order modes in circular fibers," IEEE Photonics Technol. Lett. **19**(16), 1266–1268 (2007).
24. F. W. Sheu, H. Y. Wu, and S. H. Chen, "Using a slightly tapered optical fiber to attract and transport microparticles," Opt. Express **18**(6), 5574–5579 (2010).
25. L. N. Ng, M. N. Zervas, J. S. Wilkinson, and B. J. Luff, "Manipulation of colloidal gold nanoparticles in the evanescent field of a channel waveguide," Appl. Phys. Lett. **76**(15), 1993–1995 (2000).
26. A. H. J. Yang, S. D. Moore, B. S. Schmidt, M. Klug, M. Lipson, and D. Erickson, "Optical manipulation of nanoparticles and biomolecules in sub-wavelength slot waveguides," Nature **457**(7225), 71–75 (2009).
27. C. D. Mellor, T. A. Fennerty, and C. D. Bain, "Polarization effects in optically bound particle arrays," Opt. Express **14**(21), 10079–10088 (2006).
28. K. Grujic, O. G. Hellesø, J. P. Hole, and J. S. Wilkinson, "Sorting of polystyrene microspheres using a Y-branched optical waveguide," Opt. Express **13**(1), 1–7 (2005).
29. D. Guo, L. Wu, H. Yu, A. Zhou, Q. Li, F. Mumtaz, C. Du, and W. Hu, "Tapered multicore fiber interferometer for refractive index sensing with graphene enhancement," Appl. Opt. **59**(13), 3927–3931 (2020).
30. D. A. M. Arrioja and J. R. G. Sepulveda, "Highly sensitive fiber optic refractive index sensor using multicore coupled structures," J. Lightwave Technol. **35**(13), 2695–2701 (2017).